Multiobjective System Level Optimization Method for Switched Reluctance Motor Drive Systems Using Finite Element Model

Kaikai Diao, *Student Member, IEEE*, Xiaodong Sun, *Senior Member, IEEE*,
Gang Lei, *Member, IEEE*, Youguang Guo, *Senior Member, IEEE*,
and Jianguo Zhu, *Senior Member, IEEE*

***Abstract*—This paper presents a novel multiobjective system level optimization method to achieve the best performance of switched reluctance motor (SRM) drive systems. First, the multiobjective optimization problem for the SRM drive systems is defined. Then, all parameters of the drive systems, including the motor level and control level are divided into three subspaces according to their influences on the objectives. Finally, the optimization of each subspace is performed sequentially until a convergence criterion is met. Then, the optimal solution can be chosen from the Pareto solutions according to a selection criterion. Meanwhile, the sensitivity analysis, the approximate models, and the genetic algorithm are employed to reduce the computation cost. To verify the effectiveness of the proposed method, a SRM drive system with a segmented-rotor switched reluctance motor (SSRM) and the angle position control method is investigated. This is a high-dimensional system level optimization problem with ten parameters. The finite element model (FEM) results are verified by the experiment results. The optimal solution has been listed and verified by the FEM. From the discussion, it can be found that the proposed optimization method is efficient and optimized SSRM drive has high efficiency and low torque ripple.**

***Index Terms*—Angle position control, finite element method, multiobjective optimization, switched reluctance motor, system level design optimization.**

Manuscript received June 25, 2019; revised October 6, 2019 and November 21, 2019; accepted December 19, 2019. This work was supported by the National Natural Science Foundation of China under Project 51875261, the Natural Science Foundation of Jiangsu Province of China under Projects BK20180046 and BK20170071, the "Qinglan project" of Jiangsu Province, the Key Project of Natural Science Foundation of Jiangsu Higher Education Institutions under Project 17KJA460005, and the Six Categories Talent Peak of Jiangsu Province under Pro-ject 2015-XNYQC-003. (Kaikai Diao and Xiaodong Sun equally contributed to this work.) (*Corresponding author: Xiaodong Sun.*)

K. Diao and X. Sun are with the Automotive Engineering Research Institute, Jiangsu University, Zhenjiang 212013, China (email: diaokaikai@163.com, xdsun@ujs.edu.cn).

G. Lei and Y. Guo are with the School of Electrical and Data Engineering, University of Technology Sydney, NSW 2007, Australia (e-mail: Gang.Lei@uts.edu.au, Youguang.Guo-1@uts.edu.au).

J. Zhu is with the School of Electrical and Information Engineering, University of Sydney, NSW, 2006, Australia (e-mail: jianguo.zhu@sydney.edu.au).

I. Introduction

Due to the absence of any windings and magnets in the rotor, the switched reluctance motors (SRMs) provides the best alternatives for the other machines under harsh environments of extremely high temperatures and pressures [1], [2]. However, the radial vibration influences the trade-off to the widespread application of SRMs in some specific fields, such as electric vehicles (EVs) and hybrid electric vehicles (HEVs) [3], [4].

Motor topology development and optimization are two main aspects to improve the overall performance of SRMs. In recent years, a variety of novel structures of SRMs have been presented, such as linear SRM [5], segmented stator SRM [6], double-stator SRM [7], and axial-flux SRM [8]. Previous researches on SRM system design and optimization mainly focus on one objective, such as torque ripple, torque density or efficiency. However, this single-objective optimization potentially influences the other important performance indices. Therefore, the trade-offs to the overall consideration and the implementation of multiobjective optimization are necessary to meet the requirements for different applications [9], [10]. Furthermore, previous works are mostly on the component level rather than the system level [11], [12]. Theoretically, assembling individually optimized components into a system cannot guarantee the optimal system performance as each part is coupled to each other. Thus, the perfect cooperation of motor and control levels should be optimized simultaneously.

The first step in the design optimization of an SRM is to build the analysis model for the performance parameters. Two criterions to evaluate the created model are the accuracy and computational speed. Commonly, there are mainly three kinds of analysis model, namely, finite element analysis (FEA) [13], [14], curve-fitting method [15], and magnetic equivalent circuit (MEC) method [16]. FEA is the most popular numerical analysis method. The merit of FEA is that it can provide a comprehensive and accurate solution for the nonlinear problems. However, it may not be appropriate to the optimization of motors with complex structures and high dimensions, due to the expensive computation cost of FEA. As an alternative, several surrogate models, such as Kriging model [17], response surface model (RSM) [18], radial basis functions model (RBF) [19], and artificial neural network model, have

been employed to reduce the FEA computation cost and improve the efficiency. As the flux linkage of the SRM is nonlinear with respect to both current value and rotor position, the curve-fitting method approximates the flux linkage profile with mathematical expressions or intelligent models. The main drawbacks of curve-fitting method are that they are empirical and they still require the data from FEA or experiments. MEC method is analogous to an electric circuit where the reluctances of each component of the SRM are analyzed and determined. It has fast computational speed but lacks the accuracy due to its assumptions on the magnetic flux paths [20].

The second step is to find the optimal solutions for the optimization problems. In the past two decades, various intelligent algorithms, such as genetic algorithm [21], particle swarm optimizer [22], and differential evolution algorithm (DEA) [23], have been implemented in the optimization process.

On the other hand, a variety of control methods have been proposed for the SRMs, such as conventional current chopping control [24], angle position control (APC) [25], direct torque control [26], and model predictive control [27]. However, they are only optimized on the control level for the designed SRMs due to the largely increased number of optimization parameters at the very first stage of the design and optimization of SRM drive system.

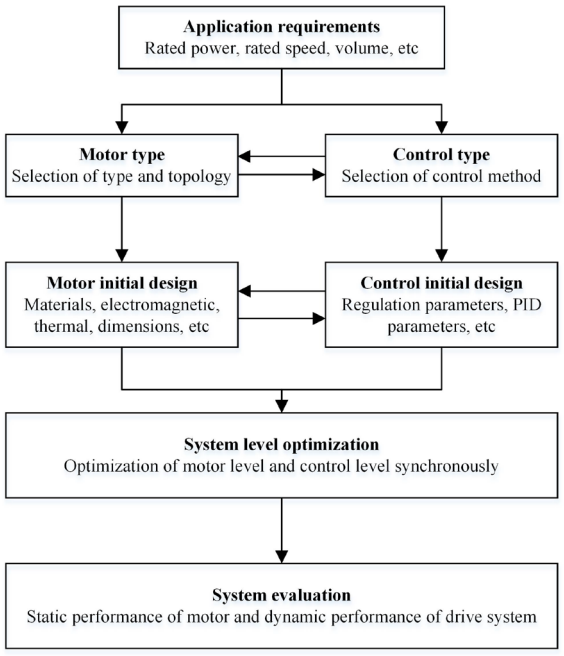

Fig. 1. System level design and optimization framework for electrical drive systems.

Coupling the control aspect with the electromagnetic part is beneficial to achieve the best performance of the SRM drive system. Although the system level optimization method of drive system has been proposed in [11], the coupled effects on the motor and control levels actually were not considered synchronously when this method was applied to a direct drive system of permanent-magnet transverse flux machine. Besides, it is a single-objective optimization method which has taken into several performances. Moreover, aside from the motor level, multiobjective optimization method has also been applied in the control sides of SRMs. The PI controller gains, and turn-on and turn-off angles can be optimized by DEA to reduce the torque ripple and improve the output torque [28]. However, few examples about multiobjective optimization considering drive system applied to the SRMs have been reported.

This paper presents a novel multiobjective system level optimization method for SRM drive systems. Both the motor and control aspects are optimized by the multiobjective optimization method. Besides, the sequential subspace optimization method is performed to reduce the computation cost and improve the optimization efficiency. The remainder of this paper is organized as follows. Section II presents the proposed method. Section III investigates an example study for the design optimization of a segmented-rotor switched reluctance motor (SSRM) and its control approach. Specific implementation and results are provided in Section IV, followed by the conclusion in Section V.

II. Multiobjective System Level Optimization Method

A. Summarization of system level optimization method

Fig. 1 shows a brief framework for the system level design optimization of electrical drive systems. This kind of system level design optimization method has taken the motor and its control system into consideration simultaneously. It can be divided into the following five steps.

Step 1: Determine the application requirements for the motor drive system.

The specific requirements of the motor system are determined by the applications. It contains many factors, such as rated power, rated speed, volume, and efficiency.

Step 2: According to the application requirements, select the motor and control type for the drive system.

In this stage, the coupled influences between multi-physics and the control aspects are taken into consideration at the same time. For most industrial and domestic applications, there are many trade-offs among different motor types. All the advantages as well as drawbacks should be thoroughly considered based on the operation conditions, cooling capabilities, torque density and the total cost. There are many applications where SRMs are considered as the best alternatives due to their low cost, superior thermal and mechanical robustness. Nowadays, the applications of SRMs in EV/HEVs, aircraft, and wind generators are the three main research aspects. The works presented in [1] proved that SRM exhibits better high-speed performance than the Prius motor. The SRMs designed for the aerospace and wind power generation are presented in [29] and [30], respectively.

Step 3: Accomplish the initial designs for both the motor and control types.

Most design approaches rely on the existed theories and FEA method. The design process of SRMs is inherently empirical

due to its high nonlinear characteristics, and there is no general mathematical model that can represent SRM performance accurately. Safety margins of critical machine parameters, such as current density and cooling capability, and the slot fill coefficient are often employed to prevent overheating and assembly difficulty, which limits the designed machine to the ideal state.

Step 4: Optimize the models for the whole system, including the motor level and control level.

The optimization problem can be defined as [11]

$$\begin{aligned} \min: \quad & f(\mathbf{x}_s) \\ s.t. \quad & g_i(\mathbf{x}_s) \le 0, i = 1,2,...,n \\ & \mathbf{x}_{sl} \le \mathbf{x}_s \le \mathbf{x}_{su} \end{aligned} \tag{1}$$

where $\mathbf{x}_s$, f, g_i are the design parameter vector, objective and constraints of motor, respectively, $\mathbf{x}_s$ consists of motor parameter vector and control parameter vector, $\mathbf{x}_{sl}$ and $\mathbf{x}_{su}$ are the lower boundary and upper boundary, respectively.

There are two strategies for the optimization of model (1), single space and sequential subspace strategies. The single space strategy optimizes all motor and control parameters simultaneously by using an algorithm like GA and DEA. It requires huge computation cost of FEA and control simulation as (1) is normally a high-dimensional optimization problem (dimension usually no less than 10). To improve the optimization efficiency, a sequential subspace optimization strategy was presented for electrical drive systems [11], [12].

Step 5: Evaluation of system's performance.

This step can be divided into two aspects, i.e., static performance of the motor and dynamic performance of the whole system. The static performance of SRMs can reflect the characteristics of motor topology and the dynamic performance of drive system can evaluate the integration of the motor and control.

B. Multiobjective optimization of SRM drive systems

Fig. 2 shows the flowchart of the proposed multiobjective system level optimization method for SRM drive systems. This method includes multiobjective, sequential subspace and system level optimizations, and it can be divided into seven steps as follows.

Step 1: Build the multiobjective optimization problem considering the system parameters for the SRM drive systems, and determine the selection criterion to choose the optimal solution.

The multiobjective model can be defined as

$$\begin{aligned} \min: \quad & \begin{cases} f_1(\mathbf{x}_s) \\ f_2(\mathbf{x}_s) \\ \vdots \\ f_m(\mathbf{x}_s) \end{cases} \\ s.t. \quad & g_i(\mathbf{x}_s) \le 0, i = 1,2,\ldots n \\ & \mathbf{x}_{sl} \le \mathbf{x}_s \le \mathbf{x}_{su} \end{aligned} \tag{2}$$

And the selection criterion can be defined as

$$\min: \quad F\{f_1(\mathbf{x}_s), f_2(\mathbf{x}_s), ..., f_m(\mathbf{x}_s)\} \tag{3}$$

For the multiobjective optimization, the objectives are conflicting to each other in most design situations [31]. The improvement of one objective may cause the decrease of the other objectives. The Pareto front as a set of non-dominated solutions is a good choice to show the optimal solutions of multiobjective optimization.

Step 2: Carry out sensitivity analysis for all parameters of the SRM drive system, including motor level and control level.

Sensitivity analysis is suitable for the high dimensional optimization problems to further divide all the parameters into different levels. As optimizing all the parameters in one subspace is time-consuming and common approximate methods lack sufficient accuracy in high dimensional problems, this method contributes to reducing the computing cost and building the approximate models. Four types of sensitivity analysis methods are commonly used, i.e., local sensitivity analysis, global sensitivity analysis, sizing equation, and analysis of variance.

Step 3: Divide the system parameters into three subspaces X_1, X_2, and X_3, where X_1, X_2, and X_3 represent the highly significant, significant, and non-significant subspaces of system design parameters, respectively.

The principle of the division is decided by the results of influences on the defined optimization objectives in (2). The results can be achieved from the sensitivity analysis or the design experience.

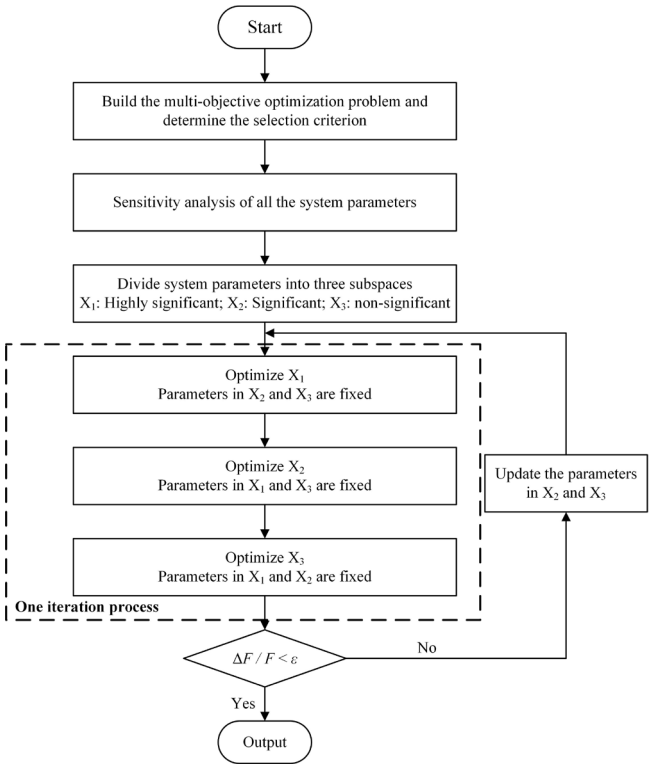

Fig. 2. Flowchart of multiobjective system level optimization method for SRM drive systems.

Step 4: Optimize subspace X_1.

In the implementation, parameters in X_2 and X_3 are fixed as the initial values at the first iteration. The approximate models and intelligent algorithms are applied in the optimization process. Firstly, develop a parametric finite element model (FEM) in X_1 for the investigated SRM and implement the simulation by using a design of experiment (DoE) technique. Secondly, obtain the simulation results and evaluate the motor performance. Thirdly, build an approximate model based on the obtained results and motor performance. This approximate model can reduce the computational cost greatly. Finally, an intelligent algorithm is employed to find the optimal solutions of the motor. The Pareto optimal solution set of X_1 is obtained in this step, and then the optimal solution is selected for the optimization of the next subspace X_2 according to (3).

Step 5: Optimize subspace X_2.

Similar to the last step, the Pareto optimal solution set of X_2 is obtained in this step based on the selected values of parameters in X_1. It should be noted that in this process, the parametric FEM is related to the variables in X_2. After the development of the optimization problem and implementation of the optimization algorithm, the optimal solutions of X_2, together with those of X_1 obtained in step 4, will be sent to the optimization of the next subspace X_3.

Step 6: Optimize subspace X_3.

The values of parameters in X_1 and X_2 are fixed as selected in this step. Similarly, after the development of FEM and optimization problem, the Pareto optimal solutions set of X_3 can be achieved by using an optimization algorithm.

It should be noted that the whole optimization of X_1, X_2, and X_3 is regarded as one iteration process. After the optimization of subspace X_3, the optimal solution of this iteration can be achieved.

Step 7: Termination judgement.

Compare the objective functions between two successive iterations. If their relative error is smaller than a given value, terminate the iteration progress and output the optimization results/Pareto front. Otherwise, update the parameters in X_2 and X_3, and go to step 4 to conduct another iteration. Steps 4-7 can be regarded as a sequential optimization process.

C. Optimization techniques

1) Approximate models

Approximate models act as an alternative for FEA and MEC, which ease the computational burden. In the modeling process, the flux linkage model and the torque model can be established by the approximate models based on the data achieved form the FEA or experiment samples. Besides, in the multiobjective optimization process, the relationship between the objectives and the parameters can be expressed by the approximate models. Kriging model is superior in the modeling of local nonlinearities since it includes both mean trend and variances of the responses compared with others, such as RSM and RBF [11]. The Kriging model will be investigated in this paper.

Given n sample points $\{x_1, x_2, ..., x_n\}$ and their responses $\{y(x_1), y(x_2), \ldots, y(x_n)$, for an input $\mathbf{x}$, the response $y(\mathbf{x})$ of the Kriging model can be expressed as

$$\hat{y}(\mathbf{x}) = F(\boldsymbol{\beta}, \mathbf{x}) + z(\mathbf{x}) \tag{4}$$

where $F(\boldsymbol{\beta},\mathbf{x})$ is the regression model and $z(\mathbf{x})$ is a random error term used for the modeling of local deviation. $F(\boldsymbol{\beta},\mathbf{x})$ is represented as

$$F(\boldsymbol{\beta}, \mathbf{x}) = \beta_1 f_1(\mathrm{x}) + \cdots + \beta_p f_p(\mathrm{x}) = f(\mathbf{x})^T \boldsymbol{\beta} \tag{5}$$

The coefficients β_k are regression parameters and $f(x)$ is a known approximation model. $z(\mathbf{x})$ is usually assumed to be a vector with mean of zero, covariance σ^2, and covariance matrix cov_{ij} as

$$\mathrm{cov}_{ij} = \sigma^2 \mathbf{R}(\theta, \mathrm{x}_i, \mathrm{x}_j) \tag{6}$$

where $\mathbf{R}(\theta, x_i, x_j,)$ is the correlation model with parameters θ.

2) Optimization algorithms

In the multiobjective optimization method, the optimal solutions are actually a compromise between all the objectives. The Pareto solutions are usually obtained by optimization algorithms. Various optimization algorithms have been applied to the multiobjective optimization problems, such as multiobjective DEA, non-dominated sorting genetic algorithm (NSGA), and its improved version NSGA II. Among these, NSGA II is one of the most efficient multiobjective evolutionary algorithms and has been widely applied in industrial multiobjective optimization problems.

III. Example of a SRM drive System

In this example, an SSRM is designed for belt-driven starter/generator (BSG) application in HEVs. The specifications of SSRM are shown in Table I. A SRM drive system consisting of this SSRM and the APC control system will be investigated.

TABLE I
SPECIFICATIONS OF THE SSRM

Parameters	Unit	value
Rated power	kW	1.8
Rated speed	r/min	6000
Rated voltage	V	60
Efficiency	%	0.85
Outer diameter	mm	128
Axial length	mm	80

Fig. 3 shows the topology of the SSRM. As shown, the stator of this SSRM is composed of excited and auxiliary poles. The excited poles are wound by windings, while the auxiliary poles are only functioned as flux return paths without any windings. The rotor contains a series of discrete segmented rotors, and each component is embedded in the nonmagnetic isolator [32]. Aside from the numbers of phases, stator and rotor, the other ten parameters listed in Table II are considered as the optimization parameters, which include the parameters of motor level and control level. It should be noted that the diameter of winding is kept as a constant during the optimization process. The main reason for this assumption is that it can simplify the optimization since it is hard to reflect the change of the winding's diameter for the SRM in FEA. Meanwhile, in the practical design process of an SRM, for a specific slot fill factor, there are several feasible combinations of the diameter of winding and the number of turns. A common

practice is that select the diameter first, then determine the optimal number of turns according to the slot fill factor and other constraints. Furthermore, the influence of the winding diameter on the resistance can also be reflected by the number of turns for a given slot fill factor.

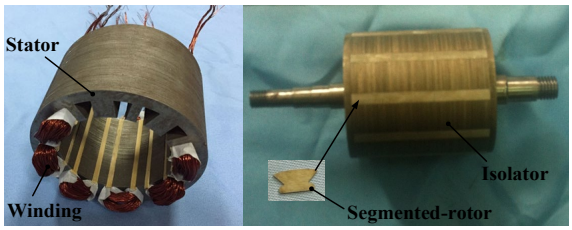

Fig. 3. Topology of the SSRM.

TABLE II
INITIAL DESIGN VALUES OF THE SSRM

Par.	Description	Unit	Value
N_{ph}	Number of phases	-	4
N_s	Number of stator poles	-	16
N_r	Number of rotor poles	-	10
D_{so}	Stator outer diameter	mm	128
l	Axial length	mm	80
D_{ro}	Rotor outer diameter	mm	82
β_{s1}	Excited stator pole arc	deg.	21.375
β_{s2}	Auxiliary stator pole arc	deg.	10.688
β_r	Rotor pole arc	deg.	26.64
L_{sy}	Stator yoke	mm	7
h_{cr}	Height of segmented rotor	mm	5.5
g	Air gap	mm	0.25
N	Number of turns	-	24
θ_{on}	Turn-on angle	deg.	-3
θ_{off}	Turn-off angle	deg	12

For this SSRM drive system, in addition to the torque and loss, the torque ripple is another important characteristic compared to the other types of machine as it is the main obstacle for the wide application of SRMs in industry. The loss is the sum of the copper loss and iron loss. In this application, the optimization problem can be defined as follows.

$$\begin{aligned} \min: \quad & \begin{cases} f_1(\mathbf{x}_s) = -T_{avg} \\ f_2(\mathbf{x}_s) = P_{loss} \\ f_3(\mathbf{x}_s) = T_{ripple} \end{cases} \\ s.t. \quad & g_1(\mathbf{x}_s) = 0.85 - \eta \le 0 \\ & g_2(\mathbf{x}_s) = sf\text{-}0.6 \le 0 \\ & g_3(\mathbf{x}_s) = J_c\text{-}6 \le 0 \\ & \mathbf{x}_{sl} \le \mathbf{x}_s \le \mathbf{x}_{su} \end{aligned} \tag{7}$$

where T_{avg}, P_{loss} and T_{ripple} are the three optimization objectives, which represent the average output torque, average loss and torque ripple, respectively. η, P_{out}, sf and J_c represent the efficiency, output power, slot fill factor and current density, respectively. It should be noted that although $f_1(\mathbf{x}_s)$ and $f_2(\mathbf{x}_s)$ can reflect the efficiency, they do not directly show whether the efficiency meet the requirement. Besides, the specification of the efficiency is listed in Table I. Thus, it has been taken as one constraint.

To select the optimal solution for a practical application, the selection criterion is defined as

$$\min: \quad F = w_1 \frac{T_{avg\_initial}}{T_{avg}} + w_2 \frac{P_{loss}}{P_{loss\_initial}} + w_3 \frac{T_{ripple}}{T_{ripple\_initial}} \tag{8}$$

where $T_{avg\_initial}$, $P_{loss\_initial}$ and $T_{ripple\_initial}$ are the average torque, loss and torque ripple of the initial design, and w_1, w_2, and w_3 are the weight factors. In this example, w_1, w_2, and w_3 are assigned as 0.4, 0.3, and 0.3, respectively. The single objective function (8) is adopted for the determination of the convergence of Pareto front since it can provide a fast optimization process [11].

IV. IMPLEMENTATION AND RESULTS

The whole discussion of the optimization method is based on the results of finite element model (FEM). Thus, the first step is to verify the reliability of the data achieved from FEM. Second, local sensitivity analysis is carried out to divide all the parameters into different subspaces to release the burden of computation. Third, the proposed multiobjective system level optimization process is performed. Then, the accuracy of the Kriging model is verified by the FEM results. Finally, comparison between the optimal solution and the initial design is investigated, and the results are further presented and discussed.

A. Verification of FEM

Fig. 4 shows the platform for the SSRM drive system. The simulation model is established in Ansoft/Maxwell, as shown in Fig. 5. The control method is angle position control (APC) and the voltage is set as 60 V. Then, mesh generation, boundary conditions and analysis setup are determined. The torque, and copper and iron losses values can be achieved in the established FEM after computation. The comparison of output torque between simulation and measured results is shown in Fig. 6. More details, including static and dynamic performances, can be found in [32]. All the measured results can verify the effectiveness of simulation results, and further prove the reliability of the FEM. Thus, the FEM samples prepared for the optimization are reliable.

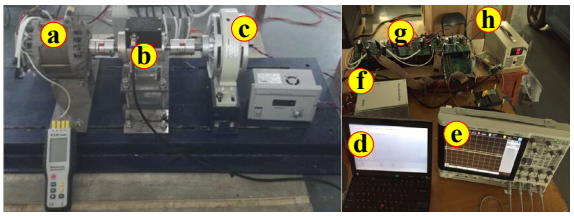

Fig. 4. Platform of the investigated SSRM drive system. (a) The 16/10 SSRM. (b) Torque and speed sensor. (c) Magnetic power brake. (d) PC. (e) Oscilloscope. (f) dSPACE. (g) Power converter and driving circuit. (h) Power supply.

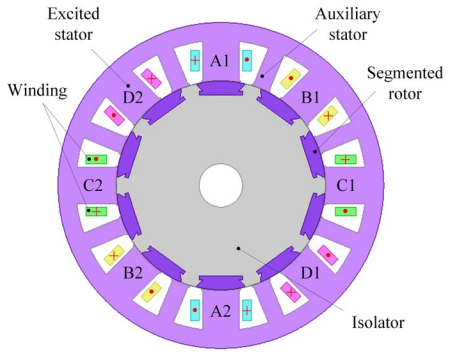

Fig. 5. The 2D FEM of the SSRM.

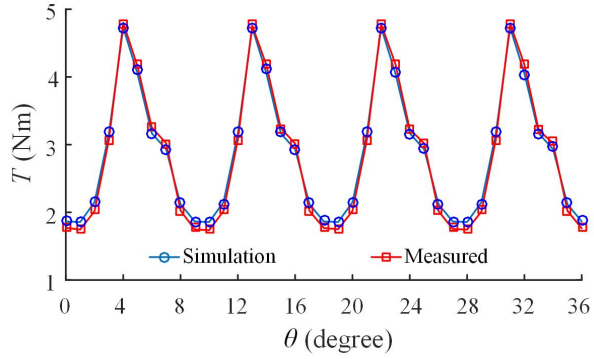

Fig. 6. Output torque comparison of the experimental and simulation results under APC at speed 6000 r/min.

B. Local sensitivity analysis

To divide all the design parameters into the proposed subspaces, the local sensitivity analysis [33], [34], which can reflect the influence/sensitivity of each parameter on the performances, are performed. Mathematically, the sensitivity of the *i*th parameter x_i at the point $\mathbf{x_0}$ can be defined as

$$S_i = \left.\frac{\partial f(\mathbf{x})}{\partial x_i}\right|_{\mathbf{x}=\mathbf{x}_0} \tag{9}$$

where S_i is the sensitivity, and $f(\mathbf{x})$ is the objective function. In this paper, $f(\mathbf{x})$ refers to torque, loss and torque ripple, respectively.

The whole sensitivity analysis is based on the FEA, and there is no accurate analytical expression of the objective function. Thus, in this case, a differential form is taken to calculate S_i.

$$S_i = \frac{f(\mathbf{x}_0 \pm \Delta\mathbf{x}_i) - f(\mathbf{x}_0)}{\pm\Delta x_i} \tag{10}$$

It should be noted that the sensitivities of different parameters calculated by (10) have different units. Thus, a normalization step considering absolute value is carried out as follows.

$$SA_i = \left|\frac{\left[f(\mathbf{x}_0 \pm \Delta\mathbf{x}_i) - f(\mathbf{x}_0)\right] / f(\mathbf{x}_0)}{\pm\Delta x_i / x_i}\right| \tag{11}$$

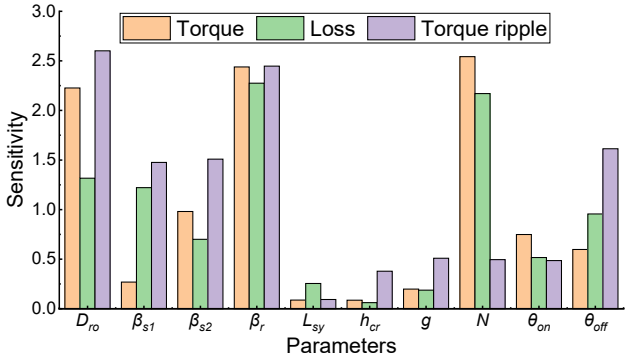

Fig. 7. Local sensitivity indices of torque, loss, and torque ripple.

In general, there are two methods to determine the increment Δx_i. The first one is the parameter variation method, in which Δx_i is usually defined as 10%, 20% or both of its initial value. The other one is known as the deviation variation method, in which Δx_i is usually defined as the standard deviation of x_i. In this paper, the first method will be investigated as the deviation is not given. It should be noted that the initial absolute value and variation range of θ_{off} are both four times those of θ_{on}, respectively, thus the local analysis of θ_{on} and θ_{off} can be referenced in this example.

The stator outer diameter and the axial length is determined by the space requirement of the application. Excluding N_{ph}, N_s, N_r, D_{so} and l, the rest ten parameters listed in Table II are considered as the optimization variables. Totally, 41 samples are required for the calculation, including 40 samples for those four variations (-20%, -10%, 10%, and 20%) and one initial sample. The four relative errors of each objective function are calculated by (6), and then the average of absolute values of these four values represents the sensitivity of the specific objective function.

Fig. 7 shows the local sensitivity analysis results of the ten parameters. Three subspaces are determined according to the sensitivity influence on the defined optimization objectives, i.e., average torque, loss and torque ripple. Subspace X_1 includes parameters D_{ro}, β_r and N, subspace X_2 includes parameters β_{s1}, β_{s2} and θ_{off}, and subspace X_3 includes parameters θ_{on}, L_{sy}, h_{cr}, and g.

C. Sequential subspace optimization

In the process of multiobjective optimization, Kriging model is used to approximate the SRM drive model, and NSGA II is selected as the optimization algorithm. For this SRM drive system, FEM is employed to calculate the torque, loss and torque ripple under APC method at the rated speed 6000 r/min. The 6000 r/min is the rated speed of the investigated SSRM; thus, the whole optimization is conducted under this speed. With the increase of the speed, the value of torque ripple decreases. Since torque ripple of SRM is directly related to the structure due to its double salient poles, the change of torque ripple has the same tendency under the whole speed range. Therefore, the value of torque ripple under fixed speed can reflect this performance of the whole speed range.

As illustrated in Fig. 2, the optimization will be terminated when the result of F defined in (8) meets the convergence criterion. In total, three iteration processes are carried out in this example where each iteration contains the sequential optimization of the three subspaces of X_1, X_2, and X_3. Figs. 8-10 show the Pareto optimal solutions of each subspace under each iteration, respectively.

The parameters in the subspace X_1 are highly significant to the overall performances of the drive system, and they are optimized at the first subspace. In this subspace, 1001 (11x13x7, where 11, 13 and 7 are the sampling numbers of parameters D_{ro}, β_r, and N, respectively) FEM samples are simulated for the optimization. After optimization of the subspace X_1, significant parameters in the subspace X_2 will be optimized under the selected values of parameters in X_1. For the optimal solution in X_1, 150 (6x5x5, where 6, 5, and 5 mean the sampling numbers of parameters β_{s1}, β_{s2} and θ_{off}, respectively) FEM samples are sampled, and the corresponding Pareto solutions can be achieved during the optimization of subspace X_2. Similarly, for the optimal solution in X_3, 180 (3x3x5x4, where 3, 3, 5 and 4 mean the numbers of values of θ_{on}, L_{sy}, h_{cr}, and g, respectively) FEM samples are required for the optimization of subspace X_3.

From Fig. 8(a), it can be found that the proposed method can provide a set of optimal solutions for situations with different output power demands. And the solution with a minimum value of F defined in (8) has been sent to the optimization of subspace X_2. In the same way, an optimal solution with a minimum value of F was sent to the next subspace. Comparing Figs. 8(a) and 8(b), the torque ripple has been reduced greatly. It means the optimization of subspace 2 can help reduce the torque ripple of the SSRM. The optimal solutions of each iteration are listed in Table III, which are shown as Iteration 1, Iteration 2 and Iteration 3. The value of ε (as illustrated in Fig. 2) is set as 1%. Since the value of $\Delta F/F$ of Iterations 2 and 3 is 0.17%, less than 1%, the optimization is terminated after three iterations.

Thus, the final optimal solution is the optimal result of the iteration 3. The value of F gradually decreases with the increase of the iteration times, as shown in Figs. 8(c), 9(c) and 10(c), and Table III.

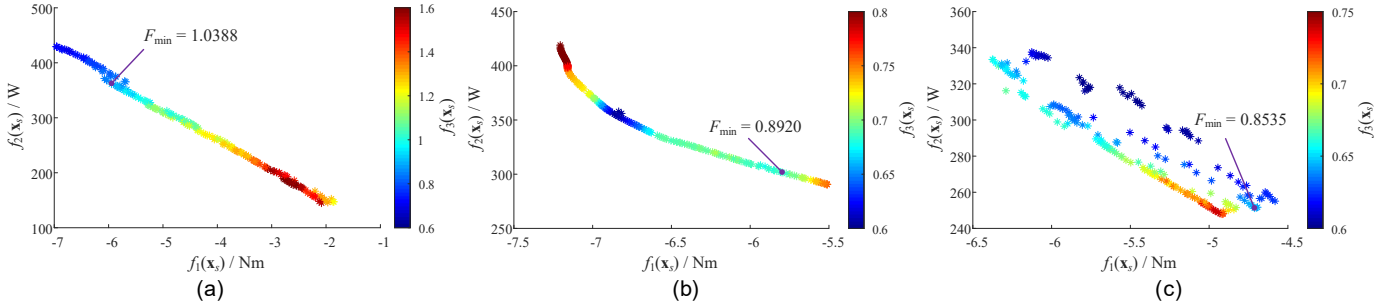

Fig. 8. Pareto optimal solutions of iteration 1. (a) Subspace X_1, (b) Subspace X_2, and (c) Subspace X_3.

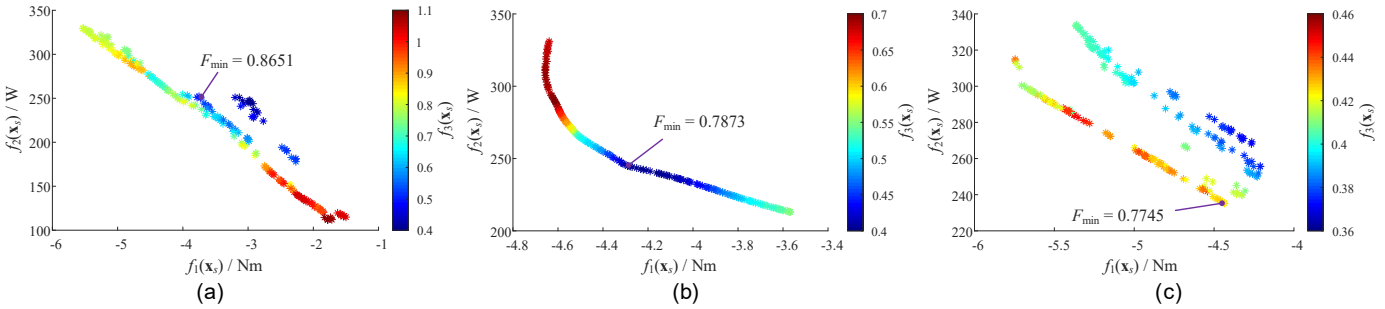

Fig. 9. Pareto optimal solutions of iteration 2. (a) Subspace X_1, (b) Subspace X_2, and (c) Subspace X_3.

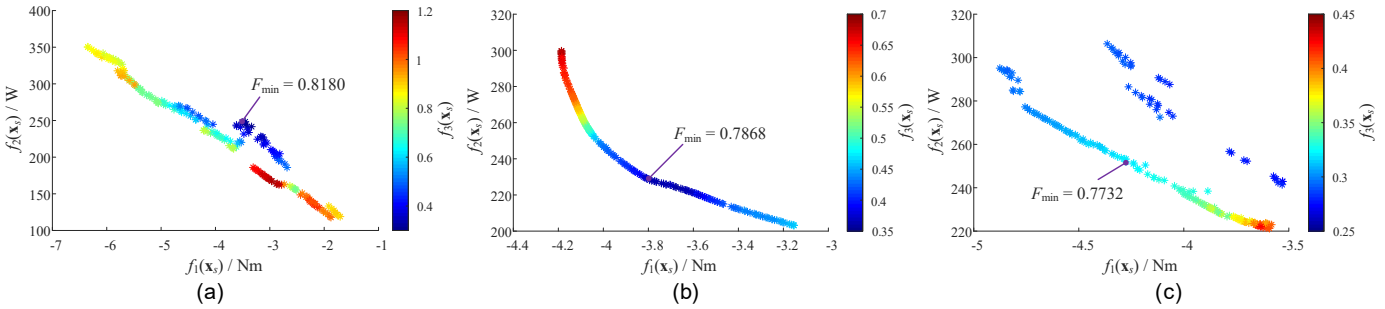

Fig. 10. Pareto optimal solutions of iteration 3. (a) Subspace X_1, (b) Subspace X_2, and (c) Subspace X_3.

TABLE III OPTIMIZATION RESULTS

Par.	Unit	Initial	Iteration 1	Iteration 2	Iteration 3
D_{ro}	mm	82.00	84.98	84.66	77.11
β_{s1}	deg.	21.38	21.50	21.50	21.50
β_{s2}	deg.	10.69	10.45	9.00	9.02
β_r	deg.	26.64	25.46	27.00	27.04
L_{sy}	mm	7.00	8.56	8.94	9.00
h_{cr}	mm	5.5	6.95	5.82	5.97
g	mm	0.25	0.3	0.25	0.25
N	-	24	20	20	20
θ_{on}	deg.	-3.00	-2.50	-2.50	-2.85
θ_{off}	deg	12.00	11.00	11.00	11.00
T_{avg}	Nm	3.03	4.72	4.43	4.30
P_{out}	kW	1.90	2.97	2.78	2.70
P_{loss}	W	195.06	250.68	235.18	252.94
η	%	90.69	92.22	92.20	91.43
T_{ripple}	%	93.64	65.03	43.44	31.94
F	-	1.00	0.8507	0.7745	0.7732

On the other hand, sequential subspace optimization can greatly improve the computational efficiency for the whole system optimization. The direct one-level optimization, for example, optimizing all ten parameters by using FEM and GA, requires around 50,000 FEM samples (500*100, where 500 is an average iteration number of GA and 100 is the population size in each iteration) are required. If Kriging model is employed, the required FEM samples (1001*150*180) will be much larger. Regarding the sequential subspace optimization, if one optimal point is selected, only 1331 (1001+150+180) FEM samples are required for one iteration in the optimization of this drive system. During the optimization process, three iteration processes are performed and totally 3993 FEM samples are required. Therefore, the proposed sequential subspace optimization method can greatly reduce the burden and cost of computation, especially for the optimization of high-dimensional structure. Besides, the computation time of each subspace is presented in Table IV, where T_FEM, T_Kriging, and T_NSGA II mean the computer time of FEM, Kriging model and NSGA II, respectively. The computation time is almost consumed by the FEM, while Kriging model and NSGA II only take up several seconds. The computation time of each iteration is the sum of the three subspaces and the final total time is the product of iteration number and the optimization time each iteration.

TABLE IV
COMPUTATION TIME OF EACH SUBSPACE

Subspace	T_FEM	T_Kriging	T_NSGA II
X_1	25 h	6.49 s	13.10 s
X_2	3.73 h	0.11 s	2.39 s
X_3	4.5 h	0.26 s	2.55 s

D. Verification of Kriging model

The Kriging model is taken to reduce the burden of computation. To ensure the optimization efficiency, it is necessary to verify the accuracy of the Kriging model. After the optimization process, the optimal solutions of each iteration are selected. Thus, the results between Kriging model and FEM of these points are compared to verify the effectiveness of the approximate model. The FEM results have been verified by the comparison with the experiment results, as mentioned above. Thus, the accuracy of Kriging model can be verified by the FEM results.

TABLE V
COMPARISON BETWEEN KRIGING MODEL AND FEM

Par.	Iteration 1		Iteration 2		Iteration 3	
	Krig.	FEM	Krig.	FEM	Krig.	FEM
T_{avg} (Nm)	4.72	4.68	4.43	4.31	4.30	4.22
P_{loss} (W)	250.68	254.77	235.18	244.57	252.94	244.32
T_{ripple} (%)	65.03	63.06	43.44	42.92	31.94	32.88
T_{avg} error	0.85%		2.71%		1.86%	
P_{loss} error	1.63%		3.99%		0.35%	
T_{ripple} error	3.03%		1.20%		1.86%	

Table V lists the values of the three optimization objectives calculated by Kriging model and FEM. As shown, the maximum errors of torque, loss, and torque ripple of these three optimal points are only 3.03%, 3.99%, and 1.86%, respectively. Thus, the accuracy of Kriging model acceptable.

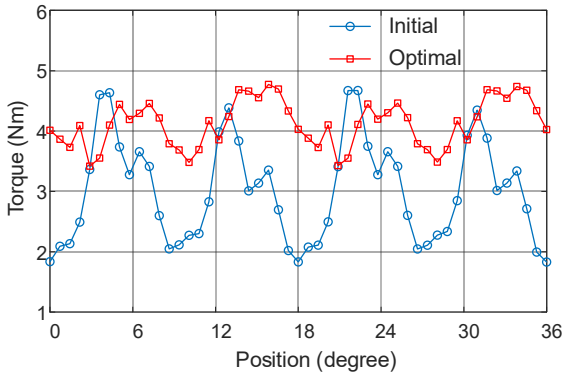

Fig. 11. Comparison of torque between the initial and optimal solutions.

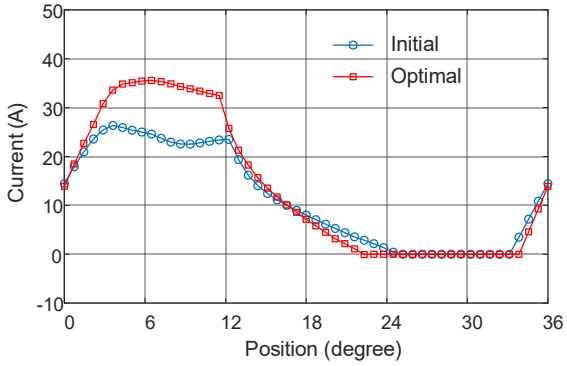

Fig. 12. Comparison of current between the initial and optimal solutions.

E. Results comparison

After verification of the Kriging model, it is credible for the optimal solutions in Figs. 8-10. The comparisons of torque and current between the optimal solution and initial design are displayed in Figs. 11 and 12, respectively. It should be noted that, to save the computation cost, the time step is 2e-5 s for the

simulation during the whole optimization process, which is twice that in Fig. 6. Thus, the simulation results between Figs. 6 and 11 may be slightly different. As shown in Fig. 11, the SSRM with the select optimal design has obvious higher average output torque and smaller torque ripple than those of the motor with the initial design. As shown in Fig. 12, compared with the initial design, the waveform of the optimal design is closer to the ideal flat waveform. Detailed comparisons of values between the initial design and the final selected optimal solution (optimum in the third iteration) are listed in Table III.

For the initial design, average torque is 3.03 Nm, efficiency is 90.69%, and torque ripple is 93.64%. After optimization of the whole system by using the proposed method, the motor's average torque reaches 4.30 Nm, which is increased by about 41.9%. The torque ripple is only 31.94%, which is reduced by about 65.89%. It means the proposed method can greatly reduce the problem of high torque ripple of SSRM drive without the sacrifice of its average torque and efficiency.

V. Conclusion

In this paper, a new multiobjective and system-level design optimization methods was presented for SRM drive systems. The proposed method aims to provide a fast way to achieve the best performance of the SRM drive system. An example of an SSRM and its APC control method was investigated to show the effectiveness of the proposed method. Three optimization objectives, i.e., torque, loss and torque ripple, were selected. To improve the overall performance of the system and reduce the computation cost, all the parameters in the design level and control level have been considered together and divided into three optimization subspaces by using the sensitivity analysis. The accuracy of the FEM and the Kriging model is verified successively. An optimal solution has been selected according to the defined selection criterion after three iteration processes. The optimal solution obtained from the proposed method exhibits many benefits for the drive system, including high efficiency and low torque ripple. In future work, different starting points and more design parameters including the winding diameter will be considered for the proposed sequential subspace optimization method. Moreover, other kinds of optimization methods, like nonlinear programming method, and other convergence criteria for the Pareto front, like hypervolume, will be investigated and compared for the multiobjective optimization of electrical drive systems.

References

[1] K. Kiyota, T. Kakishima, and A. Chiba, "Comparison of Test Result and Design Stage Prediction of Switched Reluctance Motor Competitive With 60-kW Rare-Earth PM Motor," *IEEE Trans. Ind. Electron.,* vol. 61, no. 10, pp. 5712-5721, Oct. 2014.

[2] X. Zhu, D. Fan, L. Mo, Y. Chen, and L. Quan, "Multiobjective Optimization Design of a Double-Rotor Flux-Switching Permanent Magnet Machine Considering Multimode Operation," *IEEE Trans. Ind. Electron.,* vol. 66, no. 1, pp. 641-653, Jan. 2019.

[3] S. E. Schulz and K. M. Rahman, "High-performance digital PI current regulator for EV switched reluctance motor drives," *IEEE Trans. Ind. Appl.,* vol. 39, no. 4, pp. 1118-1126, Jul./Aug. 2003.

[4] X. Sun, Y. Shen, S. Wang, G. Lei, Z. Yang, and S. Han, "Core Losses Analysis of a Novel 16/10 Segmented Rotor Switched Reluctance BSG Motor for HEVs Using Nonlinear Lumped Parameter Equivalent Circuit Model," *IEEE/ASME Trans. Mechatron.,* vol. 23, no. 2, pp. 747-757, Apr. 2018.

[5] D. Wang, X. Du, D. Zhang, and X. Wang, "Design, Optimization, and Prototyping of Segmental-Type Linear Switched-Reluctance Motor With a Toroidally Wound Mover for Vertical Propulsion Application," *IEEE Trans. Ind. Electron.,* vol. 65, no. 2, pp. 1865-1874, Feb. 2018.

[6] S. R. Mousavi-Aghdam, M. R. Feyzi, N. Bianchi, and M. Morandin, "Design and Analysis of a Novel High-Torque Stator-Segmented SRM," *IEEE Trans. Ind. Electron.,* vol. 63, no. 3, pp. 1458-1466, Mar. 2016.

[7] M. Asgar, E. Afjei, and H. Torkaman, "A New Strategy for Design and Analysis of a Double-Stator Switched Reluctance Motor: Electromagnetics, FEM, and Experiment," *IEEE Trans. Magn.,* vol. 51, no. 12, pp. 1-8, Dec., 2015.

[8] J. Ma, J. Li, H. Fang, Z. Li, Z. Liang, Z. Fu, L. Xiao, and R. Qu, "Optimal Design of an Axial-Flux Switched Reluctance Motor With Grain-Oriented Electrical Steel," *IEEE Trans. Ind. Appl.,* vol. 53, no. 6, pp. 5327-5337, Nov./Dec. 2017.

[9] X. Zhu, J. Huang, L. Quan, Z. Xiang, and B. Shi, "Comprehensive Sensitivity Analysis and Multiobjective Optimization Research of Permanent Magnet Flux-Intensifying Motors," *IEEE Trans. Ind. Electron.,* vol. 66, no. 4, pp. 2613-2627, Apr. 2019.

[10] X. Sun, Z. Shi, G. Lei, Y. Guo, and J. Zhu, "Analysis and Design Optimization of a Permanent Magnet Synchronous Motor for a Campus Patrol Electric Vehicle," *IEEE Trans. Veh. Technol.,* vol. 68, no. 11, pp. 10535-10544, Nov. 2019.

[11] G. Lei, T. Wang, Y. Guo, J. Zhu, and S. Wang, "System-Level Design Optimization Methods for Electrical Drive Systems: Deterministic Approach," *IEEE Trans. Ind. Electron.,* vol. 61, no. 12, pp. 6591-6602, Dec. 2014.

[12] G. Lei, T. Wang, J. Zhu, Y. Guo, and S. Wang, "System-Level Design Optimization Method for Electrical Drive Systems—Robust Approach," *IEEE Trans. Ind. Electron.,* vol. 62, no. 8, pp. 4702-4713, Aug. 2015.

[13] B. Bilgin, A. Emadi, and M. Krishnamurthy, "Design Considerations for Switched Reluctance Machines With a Higher Number of Rotor Poles," *IEEE Trans. Ind. Electron.,* vol. 59, no. 10, pp. 3745-3756, Oct. 2012.

[14] Z. Shi, X. Sun, G. Lei, Z. Yang, Y. Guo, and J. Zhu, "Analysis and optimization of radial force of permanent magnet synchronous Hub motors," *IEEE Trans. Magn.*, to be published, doi: 10.1109/TMAG.2019.2953731.

[15] X. Sun, K. Diao, Z. Yang, G. Lei, Y. Guo, and J. Zhu, "Direct Torque Control Based on a Fast Modeling Method for a Segmented-Rotor Switched Reluctance Motor in HEV Application," *IEEE J. Emerg. Sel. Top. Power Electron.,* to be published, doi: 10.1109/JESTPE.2019.2950085.

[16] F. E. Fleming and C. S. Edrington, "Real-Time Emulation of Switched Reluctance Machines via Magnetic Equivalent Circuits," *IEEE Trans. Ind. Electron.,* vol. 63, no. 6, pp. 3366-3376, Jun. 2016.

[17] S. I. Nabeta, I. E. Chabu, L. Lebensztajn, D. A. P. Correa, W. M. d. Silva, and K. Hameyer, "Mitigation of the Torque Ripple of a Switched Reluctance Motor Through a Multiobjective Optimization," *IEEE Trans. Magn.,* vol. 44, no. 6, pp. 1018-1021, Jun. 2008.

[18] J. H. Lee, "Optimum Shape Design Solution of Flux Switching Motor Using Response Surface Methodology and New Type Winding," *IEEE Trans. Magn.,* vol. 48, no. 4, pp. 1637-1640, Apr. 2012.

[19] J. Cai, Z. Q. Deng, R. Y. Qi, Z. Y. Liu, and Y. H. Cai, "A Novel BVC-RBF Neural Network Based System Simulation Model for Switched Reluctance Motor," *IEEE Trans. Magn.,* vol. 47, no. 4, pp. 830-838, Apr. 2011.

[20] X. Sun, K. Diao, G. Lei, Y. Guo, and J. Zhu, "Real-Time HIL Emulation for a Segmented-Rotor Switched Reluctance Motor Using a New Magnetic Equivalent Circuit," *IEEE Trans. Power Electron.,* to be published, doi: 10.1109/TPEL.2019.2933664.

[21] Y. Kano, T. Kosaka, and N. Matsui, "Optimum Design Approach for a Two-Phase Switched Reluctance Compressor Drive," *IEEE Trans. Ind. Appl.,* vol. 46, no. 3, pp. 955-964, May/Jun. 2010.

[22] J. Zhang, H. Wang, L. Chen, C. Tan, and Y. Wang, "Multi-Objective Optimal Design of Bearingless Switched Reluctance Motor Based on Multi-Objective Genetic Particle Swarm Optimizer," *IEEE Trans. Magn.,* vol. 54, no. 1, pp. 1-13, Jan. 2018.

[23] V. Rallabandi, J. Wu, P. Zhou, D. G. Dorrell, and D. M. Ionel, "Optimal Design of a Switched Reluctance Motor With Magnetically Disconnected Rotor Modules Using a Design of Experiments Differential Evolution

FEA-Based Method," *IEEE Trans. Magn.,* vol. 54, no. 11, pp. 1-5, Nov. 2018.
[24] X. Deng, B. Mecrow, H. Wu, R. Martin, and Y. Gai, "Cost-Effective and High-Efficiency Variable-Speed Switched Reluctance Drives With Ring-Connected Winding Configuration," *IEEE Trans. Energy Convers.,* vol. 34, no. 1, pp. 120-129, Mar. 2019.
[25] W. Ding, S. Yang, and Y. Hu, "Development and Investigation on Segmented-Stator Hybrid-Excitation Switched Reluctance Machines With Different Rotor Pole Numbers," *IEEE Trans. Ind. Electron.,* vol. 65, no. 5, pp. 3784-3794, May 2018.
[26] S. K. Sahoo, S. Dasgupta, S. K. Panda, and J. Xu, "A Lyapunov Function-Based Robust Direct Torque Controller for a Switched Reluctance Motor Drive System," *IEEE Trans. Power Electron.,* vol. 27, no. 2, pp. 555-564, Feb. 2012.
[27] X. Li and P. Shamsi, "Model Predictive Current Control of Switched Reluctance Motors With Inductance Auto-Calibration," *IEEE Trans. Ind. Electron.,* vol. 63, no. 6, pp. 3934-3941, Jun. 2016.
[28] X. D. Xue, K. W. E. Cheng, and S. L. Ho, "Optimization and Evaluation of Torque-Sharing Functions for Torque Ripple Minimization in Switched Reluctance Motor Drives," *IEEE Trans. Power Electron.,* vol. 24, no. 9, pp. 2076-2090, Sep. 2009.
[29] J. B. Bartolo, M. Degano, J. Espina, and C. Gerada, "Design and Initial Testing of a High-Speed 45-kW Switched Reluctance Drive for Aerospace Application," *IEEE Trans. Ind. Electron.,* vol. 64, no. 2, pp. 988-997, Feb. 2017.
[30] X. Liu, K. Park, and Z. Chen, "A Novel Excitation Assistance Switched Reluctance Wind Power Generator," *IEEE Trans. Magn.,* vol. 50, no. 11, pp. 1-4, Nov. 2014.
[31] H. Chen, W. Yan, J. J. Gu, and M. Sun, "Multiobjective Optimization Design of a Switched Reluctance Motor for Low-Speed Electric Vehicles With a Taguchi–CSO Algorithm," *IEEE/ASME Trans. Mechatron.,* vol. 23, no. 4, pp. 1762-1774, Aug. 2018.
[32] X. Sun, K. Diao, G. Lei, Y. Guo, and J. Zhu, "Study on Segmented-Rotor Switched Reluctance Motors With Different Rotor Pole Numbers for BSG System of Hybrid Electric Vehicles," *IEEE Trans. Veh. Technol.,* vol. 68, no. 6, pp. 5537-5547, Jun. 2019.
[33] J. Morio, "Global and local sensitivity analysis methods for a physical system," *Eur. J. Phys.,* vol. 32, no. 6, pp. 1577-1583, Nov. 2011.
[34] G. Lei, C. Liu, J. Zhu, and Y. Guo, "Techniques for Multilevel Design Optimization of Permanent Magnet Motors," *IEEE Trans. Energy Convers.,* vol. 30, no. 4, pp. 1574-1584, Dec. 2015.

Kaikai Diao (S'18) was born in Zhenjiang, Jiangsu, China, in 1994. He received the B.S. degree in vehicle engineering from Jiangsu University, Zhenjiang, China, in 2017, and he is currently working toward the Ph.D. degree in Jiangsu University, Zhenjiang, China.

His current research interests include design, optimization, magnetic equivalent circuits modeling, control, and loss analysis of switched reluctance motors for automobile application.

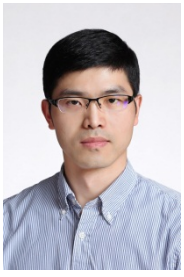

Xiaodong Sun (M'12-SM'18) received the B.Sc. degree in electrical engineering, and the M.Sc. and Ph.D. degrees in control engineering from Jiangsu University, Zhenjiang, China, in 2004, 2008, and 2011, respectively.

Since 2004, he has been with Jiangsu University, where he is currently a Professor with the Automotive Engineering Research Institute. From 2014 to 2015, he was a Visiting Professor with the School of Electrical, Mechanical, and Mechatronic Systems, University of Technology Sydney, Sydney, Australia. His current teaching and research interests include electrical machines and drives, drives and control for electric vehicles, and intelligent control. He is the author or coauthor of more than 80 refereed technical papers and one book, and he is the holder of 36 patents in his areas of interest.

Gang Lei (M'14) received the B.S. degree in Mathematics from Huanggang Normal University, China, in 2003, the M.S. degree in Mathematics and Ph.D. degree in Electrical Engineering from Huazhong University of Science and Technology, China, in 2006 and 2009, respectively. He is currently a senior lecturer at the School of Electrical and Data Engineering, University of Technology Sydney (UTS), Australia. His research interests include design optimization and control of electrical drive systems and renewable energy systems.

Youguang Guo (S'02-M'05-SM'06) received the B.E. degree from Huazhong University of Science and Technology, China in 1985, the M.E. degree from Zhejiang University, China in 1988, and the Ph.D. degree from Sydney University of Technology, (UTS), Australia in 2004, all in electrical engineering. He is currently a Professor at the School of Electrical and Data Engineering, University of Technology Sydney (UTS). His research fields include measurement and modeling of properties of magnetic materials, numerical analysis of electromagnetic field, electrical machine design optimization, power electronic drives and control.

Jianguo Zhu (S'93–M'96–SM'03) received the B.E. degree in 1982 from Jiangsu Institute of Technology, Jiangsu, China, the M.E. degree in 1987 from Shanghai University of Technology, Shanghai, China, and the Ph.D. degree in 1995 from the University of Technology Sydney (UTS), Sydney, Australia, all in electrical engineering. He was appointed a lecturer at UTS in 1994 and promoted to full professor in 2004 and Distinguished Professor of Electrical Engineering in 2017. At UTS, he has held various leadership positions, including the Head of School for School of Electrical, Mechanical and Mechatronic Systems and Director for Centre of Electrical Machines and Power Electronics. In 2018, he joined the University of Sydney, Australia, as a full professor and Head of School for School of Electrical and Information Engineering. His research interests include computational electromagnetics, measurement and modelling of magnetic properties of materials, electrical machines and drives, power electronics, renewable energy systems and smart micro grids.